Discharge studies in Micromegas detectors in low energy hadron beams

G. Charles[a], M. Anfreville[b], S. Aune[b], J. Ball[a], Y. Bedfer[a], M. Boyer[b], P. Konczykowski[a], F. Kunne[a], C. Lahonde-Hamdoun[b], L. Cai[a], I. Mandjavidze[b], C. Marchand[a], O. Meunier[b], B. Moreno[a], H. Moutarde[a], D. Neyret[a], A. Obertelli[a], S. Procureur[*,a], F. Sabatié[a], M. Vandenbroucke[a]

[a] *CEA, Centre de Saclay, Irfu/SPhN, 91191 Gif sur Yvette, France.*
[b] *CEA, Centre de Saclay, Irfu/Sedi, 91191 Gif sur Yvette, France.*

Abstract

We present measurements of discharge rates in various Micromegas detectors in low energy hadron beams for applications foreseen at the future experiments CLAS12 at JLab and MINOS at GSI. The tests were performed in the T11 beam line of the CERN/PS using hadron beams with momentum between 0.2 and 3 GeV/c. The discharge probability decreases smoothly below 1 GeV/c, except at some specific energies where narrow peaks are observed. The position of the peaks corresponds to the stop point of protons and heavier particles, predicted by the Geant4 simulation. Discharge rates were also measured using Micromegas prototypes equipped with a GEM foil as foreseen for the COMPASS experiment at CERN.

Key words: Micro Pattern Gaseous Detectors, Micromegas, GEM, Discharge, Spark, CLAS12, COMPASS, MINOS, Geant4
PACS: 29.40.Cs, 29.40.Gx

1. Introduction

Since its invention in 1996, the Micromegas detector [1] has been studied extensively and widely used in high energy physics. Its ability to withstand high fluxes of particles combined with a low material budget and excellent performance makes it very attractive for modern particle physics experiments. Other characteristics, such as its robustness and low price, were further improved with the *bulk* manufacturing process [2] developed in 2006. Thanks to this new process thin and flexible detectors can now be built and used in cylindrical shape as needed for the future trackers of CLAS12 [3] and MINOS [4] spectrometers, devoted respectively to the study of the nucleon structure and of exotic nuclei. The current limitation of Micromegas mainly comes from the generation of a

[*] *Email address*: Sebastien.Procureur@cea.fr.

large number of electron-ion pairs in the gas volume, which can lead to a discharge (or spark) between the micro-mesh and the readout strips. This situation usually occurs with the stopping of highly ionizing particles, coming either from the incident beam or from nuclear interactions in the detector's material [5]. Many studies have already been performed on discharge rates in hadron beams [6, 7], however only at momenta above 5 GeV/c. Measurements below a few GeV/c, needed for the CLAS12 and MINOS experiments are still lacking. In the case of CLAS12, the hadron flux is expected to be of the order of 1 MHz per detector, with more than 90% of hadrons between 0.1 and 1 GeV/c.

2. Experimental setup

2.1. Beam line

The tests took place in the T11 beam line of the CERN Proton Synchroton (PS) in August 2010. This line was chosen for its characteristics [8] in:

- luminosity: the discharge probability usually being of the order of one per million, a beam flux higher than 10^5 per spill is needed for precise measurements, with a beam size of a few cm^2 to match the active area of the detectors;
- energy range: the beam momentum is easily tunable from 0.2 to 3 GeV/c, and therefore covers the whole CLAS12 kinematics.

T11 delivers beam in one or two spills of 0.4 s every 50 s. Both polarities of focusing magnets can be used, leading to π^- or π^+ beams. In the latter case, a small contamination of (mainly) protons is expected. During the 2 weeks of data taking, more than 27,000 spills were delivered, corresponding to 3.8 billion particles.

2.2. Prototypes and setup

Twelve prototypes built with the bulk technology have been installed and tested simultaneously in the beam line as illustrated in Fig. 1, to compare them in the same running conditions. All the detectors were made from the same, 0.8 mm thick, Printed Circuit Board (PCB). A woven, stainless steel micro-mesh with 18 micron thick wires separated the 128 micron amplification gap from the 5 mm conversion gap. A 25 micron thick aluminized Mylar was used as the drift electrode. Their other main characteristics are summarized in Table 1. Four detectors placed at the extremities of the setup were used as reference for tracking and beam monitoring in horizontal (X) and vertical (Y) directions. Two detectors were equipped with an additional GEM foil placed respectively at 1 and 2 mm from the micro-mesh, to study the effect of the transfer gap on the discharge rate reduction. One detector was mounted on a rotating structure to measure the impact of the beam angle on the discharge probability. Two prototypes were equipped with different micro-meshes built with 16 (resp. 50) microns wires placed every 56 (resp. 265) microns. Almost all the detectors

were built at the Saclay new bulk workshop, except a reference one which was built at CERN. The same gas mixture (95% Ar - 5% iC_4H_{10} in volume) was used during all the test.
For each detector, the 140 strips with a 400 micron pitch covered an active area of 5.6×10 cm^2, and were connected to the readout electronics developed for the T2K experiment [9]. The ASIC continuously reads and filters the strip signal and samples it in an analog memory until a trigger occurs. The connection to the detectors was ensured by 150 cm long SAMTEC micro-coaxial cables, having a capacitance of 70 pF/m. The data from the twelve detectors were collected by six Front-End Cards (with four ASICs each) mounted on a T2K Front-End Mezzanine. In spite of very long cables, a S/N ratio of 30 was obtained in this configuration with minimum ionizing particles. For each trigger, 60 consecutive samples were read-out for all of the 1728 electronic channels. An acquisition rate of 150 Hz was achieved. The trigger signal was defined by the coincidence of three 15×15 cm^2 plastic scintillators, two upstream and one downstream of the detectors. This triple coincidence was also used to monitor the beam luminosity on a spill by spill basis. A systematic comparison between the triple and all the double coincidences have been performed, and concluded that the trigger efficiency is very close to 100%.

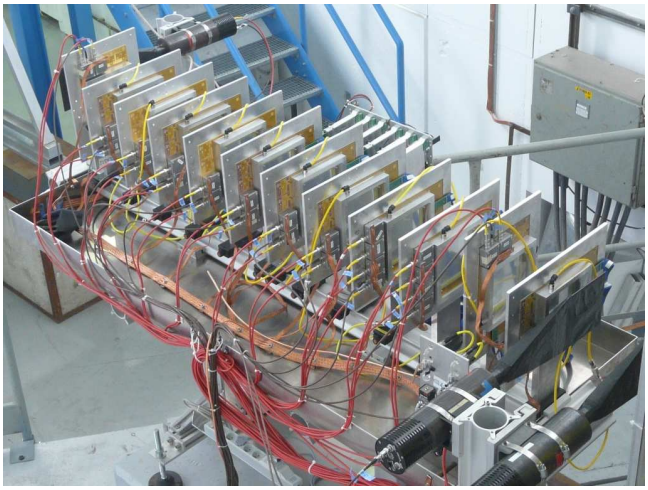

Figure 1: Picture of the experimental setup.

2.3. Discharge monitoring

Discharges in the detectors were tagged by measuring rapid changes of the micro-mesh potential through a capacitor [6]. The amplified resulting signal was sent through a discriminator to a CAEN V560N 16-channel VME scaler, and the run duration was given by a 5 Hz clock. A CAEN V2718 VME controller was used to communicate with the DAQ monitored through a LabVIEW user

position in beam	name	main characteristics
1	TFV2-01	X reference
2	TFV2-02	Y reference
3	TFV2-03 (MMGEM2)	detector with GEM foil, 2 mm transfer gap
4	TFV2-04 (MMGEM1)	detector with GEM foil, 1 mm transfer gap
5	TFV2-05	detector rotating along vertical axis
6	TFV2-07	micro-mesh 56/16
7	TFV2-08	micro-mesh 265/50 (amplification gap: 192 microns)
8	TFV1-03	resistive kapton
9	TFV2-09	drift electrode: standard or woven, stainless steel mesh
10	TFV1-04	CERN bulk
11	TFV2-06	X reference
12	TFV1-20	Y reference

Table 1: Specificity of each prototype used.

interface. The current scaler values were written at a maximum frequency of 50 Hz into an ASCII file for offline analysis.

3. Calibrations

3.1. Gain measurements

The gain of each detector was measured before the beam test as a function of the micro-mesh high voltage. The calibration was performed using a 5.9 keV X-rays from a ^{55}Fe source for which 225 primary electrons are created on average in a 95% Ar - 5% iC_4H_{10} gas mixture. The extraction of the detector's gain required a prior calibration of the acquisition chain, made through the injection of fixed voltages through a reference capacitance. Similar gains have been obtained for all non GEM detectors, as illustrated for some of them in Fig.2, except the one with a thicker micro-mesh and amplification gap.

For the two detectors mounted with a GEM foil (MMGEM) the gain was first measured without the GEM foil. A 2D fit of the gain as a function of GEM and micro-mesh high voltages was then performed for transfer fields [1] of 100 and 300 V/mm. The results are given in Fig.3.

3.2. Luminosity corrections

The estimate of the discharge probability per incident particle requires the measurement of the luminosity which is evaluated from the number of coincidences in the scintillators. However, the scintillators are larger than the detectors, and therefore trigger on more particles than seen by the detectors. This effect is emphasized at low momentum where the beam is much wider (see Fig.4).

[1] The transfer field is the field between the GEM foil and the micro-mesh.

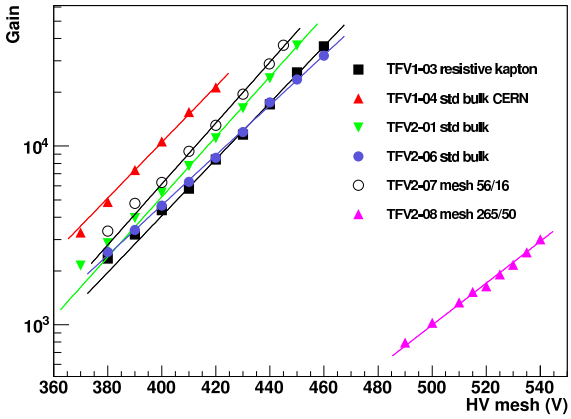

Figure 2: Gains measured as a function of the micro-mesh high voltage for some of the non GEM detectors. The detector with the smallest gains has a thicker micro-mesh and a 192 micron amplification gap.

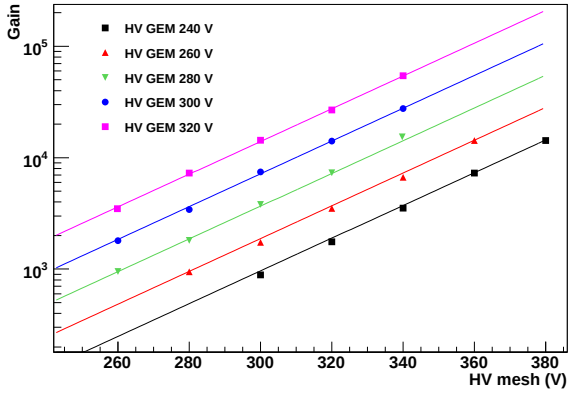

Figure 3: Gains as a function of the micro-mesh high voltage for the MMGEM with a 2 mm transfer gap. The transfer field is 100 V/mm and the GEM high voltage is varied from 240 V to 320 V.

Corrections are therefore needed to determine the number of particles going through each detector as a function of the number of coincidences between scintillators N_{coin}. The calculation proceeds in two steps:

- the 2D beam profiles in the scintillators are first estimated from the extrapolation of 1D profiles in the detectors, the latter coming from gaussian fits of the hit positions. The total number of particles in the spill N_{spill} is thus obtained;

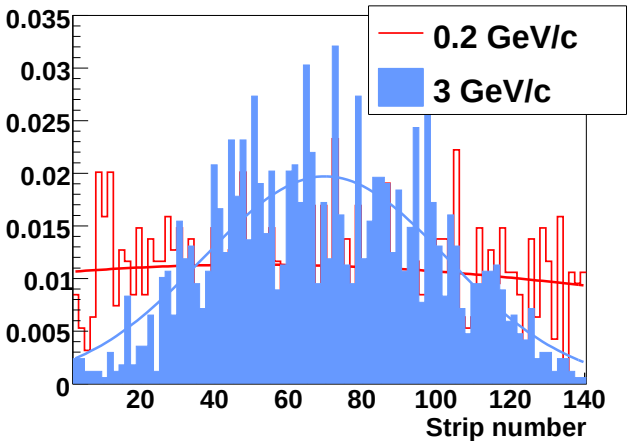

Figure 4: Distribution of the hit position in the most upstream detector using 3 GeV/c (full) and 0.2 GeV/c (hollow) π^- beam. The two curves are gaussian fits.

- the number of particles $N_{det\ i}$ crossing the i^{th} detector for each spill is then calculated from the gaussian profile in the detector.

This leads to the following relations:

$$N_{spill} = N_{coin} \cdot \frac{\iint\limits_{\mathbb{R}} g(\mu_x, \sigma_x, \mu_y, \sigma_y)}{\iint\limits_{Sc} g(\mu_x, \sigma_x, \mu_y, \sigma_y)}, \tag{1}$$

where g is the 2D normalized gaussian beam profile, μ_x, μ_y, σ_x and σ_y are the average positions and the spreads of the beam profiles in X and Y directions. $\iint\limits_{Sc}$ stands for the integration on the scintillators paddles area.
The number of particles crossing the detector i is similarly calculated as:

$$N_{det\ i} = N_{spill} \cdot \frac{\iint\limits_{det\ i} g(\mu_{x,det\ i}, \sigma_{x,det\ i}, \mu_{y,det\ i}, \sigma_{y,det\ i})}{\iint\limits_{\mathbb{R}} g(\mu_{x,det\ i}, \sigma_{x,det\ i}, \mu_{y,det\ i}, \sigma_{y,det\ i})}, \tag{2}$$

where $\mu_{det\ i}$ and $\sigma_{det\ i}$ are the mean position and the spread for the i^{th} detector. By combining Eq. 1 and Eq. 2, the number of particles crossing the detector i can be expressed as:

$$N_{det\ i} = N_{coin} \cdot \frac{\iint\limits_{\mathbb{R}} g(\mu_x, \sigma_x, \mu_y, \sigma_y)}{\iint\limits_{Sc} g(\mu_x, \sigma_x, \mu_y, \sigma_y)} \cdot \frac{\iint\limits_{det\ i} g(\mu_{x,det\ i}, \sigma_{x,det\ i}, \mu_{y,det\ i}, \sigma_{y,det\ i})}{\iint\limits_{\mathbb{R}} g(\mu_{x,det\ i}, \sigma_{x,det\ i}, \mu_{y,det\ i}, \sigma_{y,det\ i})} \equiv N_{coin} \cdot C \tag{3}$$

C is defined as the luminosity correction factor, and varies between 0 (high correction) and 1 (small correction). The values obtained are presented in Fig.

5. As expected the correction is close to one at 3 GeV/c, where the beam is better focused. It corresponds to a number of particles per spill of the order of 2×10^5. The calculated correction factor evolves smoothly with the beam momentum. It is fitted by $\alpha_i + \beta_i/p^{0.4}$, where α_i and β_i are the fit parameters for the ith detector and p is the beam momentum. The fit is then used to correct for the luminosity. As expected the two fits are very similar, since the two beams differ only by the direction of the magnetic field in the magnets of the T11 beam line [2].

Different fitting functions were tried to estimate the systematics associated

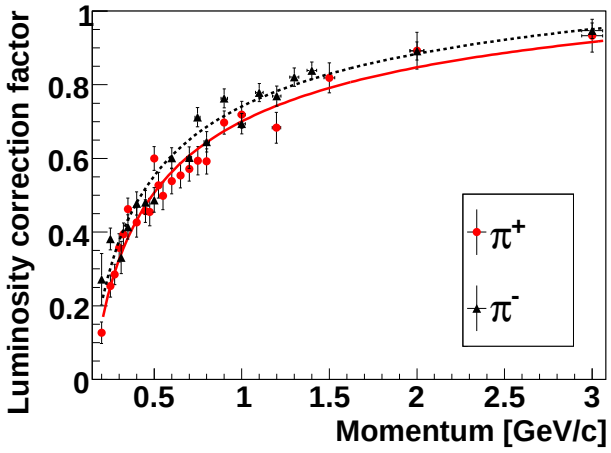

Figure 5: Luminosity correction factor (C) for one detector, as a function of the beam momentum, calculated with π^+ and π^- data. The curves are fits of the form $\alpha + \beta/p^{0.4}$.

with the correction factor calculation. It lead to systematic errors of the order of 5%, and up to 10 % at low momenta.

4. Discharge probability in standard Micromegas

4.1. Discharge probability as a function of particle type and momentum

The discharge probability per incident particle was measured as a function of the beam momentum, and corrected for the luminosity effect. Almost all the detectors exhibited similar discharge probabilities. This is illustrated for three of them in Fig. 6, using a micro-mesh high voltage of 430 V, corresponding to gains above 10^4. Above 1 GeV/c, the discharge probability is independent of the momentum and pion charge, and is of the order of 2×10^{-5}. This value is in agreement with a previous measurement obtained at 15 GeV/c with the same gas mixture [6]. Below 1 GeV/c however, the discharge probability slowly decreases, except at some specific momenta for which large and narrow peaks

[2]The proton contamination is too small to change the beam profile.

show up in the case of the π^+ beam. These peaks cannot be explained by any resonances in the pion cross sections. However, the π^+ beam is slightly contaminated by heavier particles, which is not the case for the π^- beam. Using a Geant4 simulation of the setup (see section 6), it appears that the position of the three peaks are well compatible with momenta for which protons, deuterons and tritons stop in the detectors. Such particle stopping leads to large energy deposits and therefore to a high discharge probability. This interpretation is confirmed by the observed shifts of the peak positions from one detector to another, caused by the energy loss in the setup.

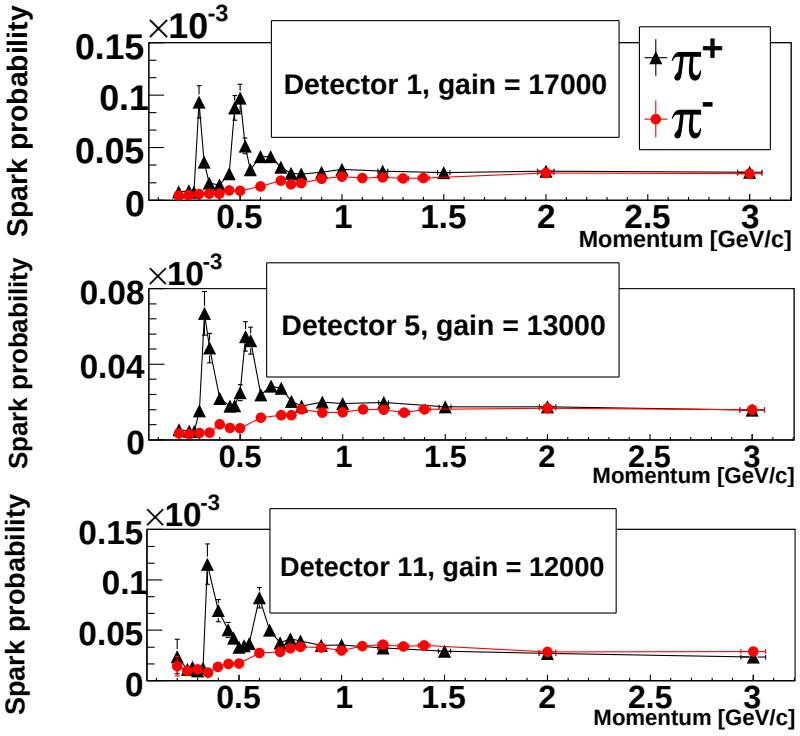

Figure 6: Discharge probability as a function of the beam momentum for π^- (circles) and π^+ (triangles) for detectors in position 1, 5 and 11. Statistical and systematic errors (from the luminosity correction factor) are included.

4.2. Discharge probability as a function of the conversion gap

During the tests, the conversion gap of one detector was varied from 2 to 5 mm to study the effect of this gap on the discharge probability. Previous tests were performed on this parameter, but no precise conclusion could be reached as they did not make use of the same detector. At a fixed gain, the discharge probability should depend only weakly on the conversion gap. According to the simulation, a small fraction of the highly ionizing particles are indeed created by

nuclear interactions with the gas volume. The result on the discharge probability is shown in Fig. 7 using 3 GeV/c π^-. No significant trend is observed within the error bars. Measurements at several different gains yield the same conclusion.

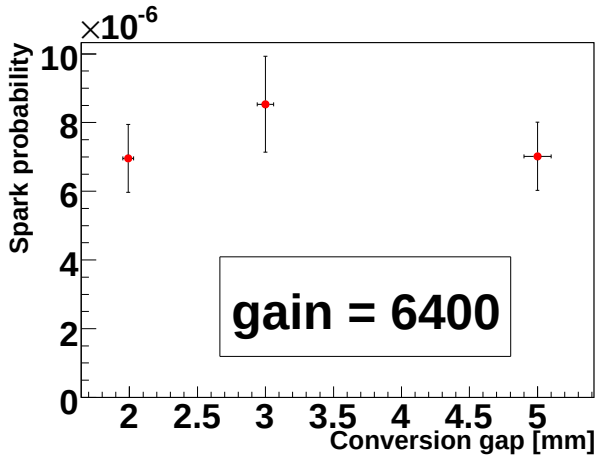

Figure 7: Discharge probability as a function of the conversion gap height for 3 GeV/c π^- beam. Statistical and systematic errors are included.

5. Discharge probability in MMGEM detectors

Previous studies showed that the discharge probability of a Micromegas equipped with a GEM foil (MMGEM) is reduced by a factor of 10 to 100 compared to a standard Micromegas at the same total gain. The reduction proved that the relevant parameter in the discharge development is not the total number of electrons, but more likely a local charge density. To better understand the effect of the transfer gap and of the GEM pre-amplification, two MMGEMs with 1 and 2 mm gaps were studied for various GEM high voltages. The measured discharge probabilities as a function of the total gain are presented in Fig. 8 and compared with a standard Micromegas using 3 GeV/c π^-. From Fig. 8.a) to 8.f) the HV difference of the GEM foil is increased by steps of 20 V starting from 240 V.

At moderate GEM gains (first two plots), a large reduction of the discharge probability is already observed compared to the standard Micromegas, but there is no significant difference between the two MMGEMs. Therefore the transverse diffusion in the transfer gap, affecting mostly the electrons created in the conversion gap, does not change the discharge probability. This suggests that the discharges occurring in this regime mainly come from large energy deposits in the transfer gap. These deposits being amplified only by the Micromegas gain, they are dramatically suppressed by transferring part of the gain to the GEM

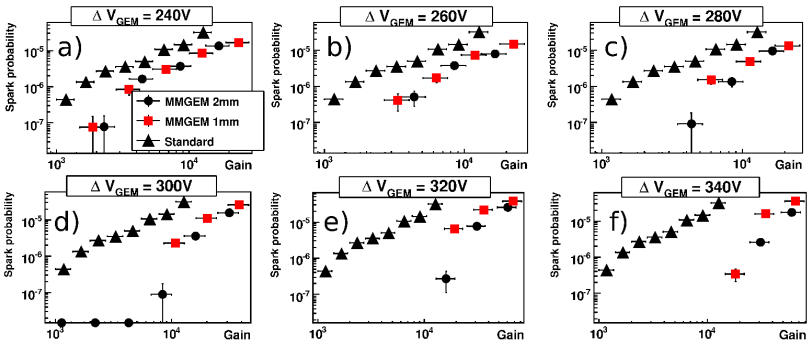

Figure 8: Discharge probability as a function of the total gain for the two MMGEMs and a standard Micromegas with 3 GeV/c π^-. From a) to f) the GEM high voltage is increased by steps of 20 V, with a constant transfer field of 300 V/mm for the two MMGEMs.

foil.
At higher GEM gains however, the discharge probability is further reduced in the MMGEM with the largest transfer gap. It indicates that the discharges originating from the transfer gap have been suppressed enough to be sensitive to discharges coming from the conversion gap. Not surprisingly, these discharges are better suppressed with a larger transverse diffusion. The relevant parameter in the development of a discharge is therefore a local charge density rather than a total number of electrons.

6. Geant4 simulation of the discharge probability

Simulations have been performed to understand the variations of the discharge rate with the beam momentum in the case of positively charged particles. In Geant4 simulations, a discharge is associated with a local, large energy deposit in the detector, as detailed in [5]. The large energy deposits occur from highly ionizing particles, usually produced from nuclear interactions between the detector material and the incident beam particles. In addition incident low energy particles can themselves be highly ionizing. For example, 290 MeV/c protons usually stop in the very first detector. In this configuration, this detector is likely to record large discharge rates. Increasing the beam momentum by a few MeV/c will lead protons to stop in the following detectors, thus leading to a very rapid increase of their discharge rate. This is exactly what is seen around 300 MeV/c (see Fig. 6) where the narrow peaks are slightly shifted in momentum from one detector to another.
Similar simulations with heavier positively charged particles show that the stopping of deuterons (resp. tritons) occurs around 500 (resp. 650) Mev/c, again very close to the momentum of the second and third peaks of Fig. 6.
The discharge probabilities obtained from the simulation for pions, protons, deuterons and tritons are shown in Fig.9 as a function of the beam momentum.

Except for pions, it is not possible to quantitatively compare with the data since the contamination of the beam with heavier particles is poorly known. The contaminations introduced in the simulation for protons, deuterons and tritons were therefore tuned to reproduce the amplitudes of the three peaks. From this tuning, it turns out that the ratio between proton and deuteron contaminations (≈ 7) is the same as between deuteron and triton, which is reasonable. Concerning protons, the tuning leads to a 0.5% contamination of the π^+ beam. This is in disagreement with an old simulation of the T11 line [8] which predicted a contamination of the order of 10%. However, systematic flux measurements performed in the scintillators located upstream and downstream of the detectors agreed within 1% even with the 300 MeV/c π^+ beam. In this configuration, protons can only be seen by the upstream scintillators, meaning that the proton contamination should be smaller than 1%. The value obtained from the tuning of the simulation agrees with this observation.
For pions, the simulation gives the correct order of magnitude for the discharge probability, using a Raether limit of 4×10^7. This limit is similar to the one used in [5], i.e. 2×10^7, and therefore confirms the ability of the simulation to predict the correct order of magnitude for the discharge rate.

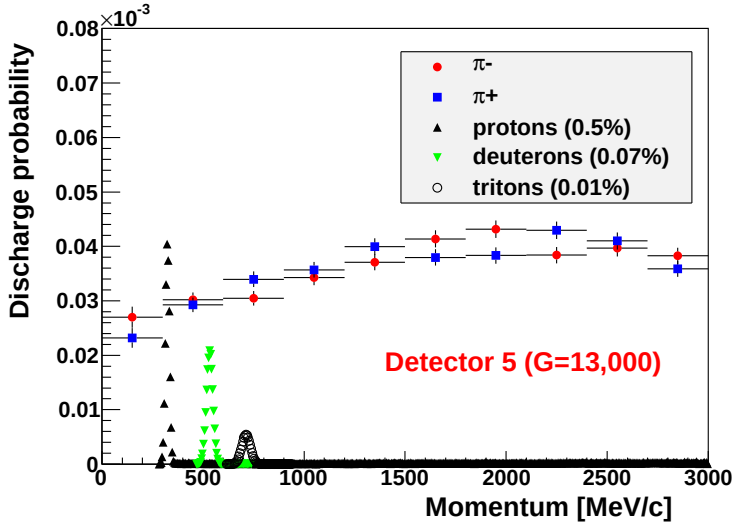

Figure 9: Geant4 simulation of the discharge probability as a function of the beam momentum obtained for different particles, in the detector 5 (with a gain of 13,000). Protons, deuterons and tritons are scaled to represent 0.5%, 0.07% and 0.01% of the $\pi+$ beam, respectively.

7. Conclusion

Measurements of discharge rates in Micromegas have been performed at beam energies between 0.2 and 3 GeV/c. Large variations of the discharge probability have been observed with $\pi+$ beam below 1 GeV/c. These variations are well described by a Geant4 simulation, confirming its reliability for discharge rate predictions. Systematic studies also lead to a better understanding of the origin of the discharge reduction in Micromegas equipped with a GEM foil. The measurements at moderate GEM gains suggest that the discharges in MMGEMs are generated mainly by large energy deposits in the transfer gap. At high GEM gains however, discharges originating from the conversion gap become predominant. In this configuration, the transverse diffusion in the transfer gap plays an important role to further reduce the discharge rates. All these results are of particular importance for the application of Micromegas detectors for high luminosity and low energy experiments.

Acknowledgments

We are particularly grateful to Lau Gatignon for useful discussions before and during these tests to optimize the setup and for the beam tuning. Special thanks are due to Horst Breuker for the dedicated beam time granted on the T11 line. We also thank J. Duplessy and B. Pichler for their help on safety issues.

References

[1] Y. Giomataris *et al.*, Nucl. Instrum. Methods A **376** (1996) 29

[2] Y. Giomataris *et al.*, Nucl. Instrum. Methods A **560** (2006) 405-408

[3] S. Aune *et al.*, Nucl. Instrum. Methods A **604** (2009) 53-55

[4] A. Obertelli, ERC-Starting Grant 2010, 258567-MINOS

[5] S. Procureur *et al.*, Nucl. Instrum. Methods A **621** (2010) 177

[6] D. Thers *et al.*, Nucl. Instrum. Methods A **469** (2001) 133

[7] S. Procureur *et al.*, submitted in Nucl. Instrum. Methods A

[8] O. Ferrando, http://gatignon.web.cern.ch/gatignon/EastArea/docs/T11_Guide.pdf

[9] P. Baron *et al.*, IEEE Trans.Nucl.Sci.55:1744-1752, 2008